



Colloidal dynamics over a tilted periodic potential: Forward and reverse transition probabilities and entropy production in a nonequilibrium steady state

Xiao-guang Ma,^{1,*} Yun Su,¹ Pik-Yin Lai,^{2,†} and Penger Tong^{1,‡}

¹*Department of Physics, Hong Kong University of Science and Technology, Clear Water Bay, Kowloon, Hong Kong*

²*Department of Physics and Center for Complex Systems, National Central University, Chungli District, Taoyuan City, Taiwan 320, Republic of China*

(Received 2 May 2017; published 7 July 2017)

We report a systematic study of the forward and reverse transition probability density functions (TPDFs) and entropy production in a nonequilibrium steady state (NESS). The NESS is realized in a two-layer colloidal system, in which the bottom-layer colloidal crystal provides a two-dimensional periodic potential $U_0(x, y)$ for the top-layer diffusing particles. By tilting the sample at an angle with respect to gravity, a tangential component of the gravitational force F is applied to the diffusing particles, which breaks the detailed balance (DB) condition and generates a steady particle flux along the [1,0] crystalline orientation. While both the measured forward and reverse TPDFs reveal interesting space-time dependence, their ratio is found to be independent of time and obeys a DB-like relation. The experimental results are in good agreement with the theoretical predictions. This study thus provides a better understanding on how entropy is generated and heat is dissipated to the reservoir during a NESS transition process. It also demonstrates the applications of the two-layer colloidal system in the study of NESS transition dynamics.

DOI: [10.1103/PhysRevE.96.012601](https://doi.org/10.1103/PhysRevE.96.012601)

I. INTRODUCTION

Detailed balance (DB) is an important principle in equilibrium statistical physics that has been used to describe the kinetics of various physical, chemical, and biological systems at thermal equilibrium. DB states that each kinetic process at equilibrium shall be equilibrated by its reverse process. Consider the probability $\Pi(x_1, x_2, \tau)$ of a forward transition from x_1 to x_2 over a time interval τ and its reversal transition probability $\Pi(x_2, x_1, \tau)$, the detailed balance condition reads [1]

$$P(x_1)\Pi(x_1, x_2, \tau) = P(x_2)\Pi(x_2, x_1, \tau), \quad (1)$$

where $P(x_1)$ and $P(x_2)$ are, respectively, the stationary probability densities at each position. Systems satisfying Eq. (1) are called microscopically reversible. The DB condition holds at equilibrium, which assures that each elementary forward process is balanced by its reverse counterpart, for any two positions x_1 and x_2 and for any transition time τ , and thus the transition probability ratio follows the Boltzmann distribution,

$$\frac{\Pi(x_1, x_2, \tau)}{\Pi(x_2, x_1, \tau)} = \frac{P_B(x_2)}{P_B(x_1)} = e^{-[U_0(x_2) - U_0(x_1)]/k_B T}, \quad (2)$$

where $U_0(x)$ is the potential energy of the system.

Nonequilibrium states, on the other hand, differ significantly from the equilibrium ones in that they often involve a net flux of mass, momentum, or heat, so that DB is broken. Experimentally, a nonequilibrium state can be generated by applying a “generalized force,” such as a gradient of concentration, temperature, velocity, or (chemical) potential, to the system. When the generalized force is a constant independent of time, the system can be driven into a nonequilibrium steady state

(NESS), which is perhaps the simplest class of nonequilibrium states [2,3]. In the NESS, entropy is produced at a positive rate on average, which is a measure of irreversibility.

While much is known about fluctuations at equilibrium, our current understanding of fluctuations in nonequilibrium states is rather limited [4]. For a NESS system consisting of a large number of particles, there are considerable fluctuations of entropy production among different particle trajectories [3,5]. These fluctuations may vary spatially in different positions owing to the complex potential landscape that the particles experience or due to strong interactions between the particles, which prevents one from treating the system as a quasiequilibrium one by simply transforming the system into a moving frame with the particle’s mean velocity [6,7]. Fluctuations in entropy production may also vary in amplitude both in the positive and negative directions. While the fluctuation theorem [8,9] predicts a universal form for the probability density function (PDF) ratio $P(\sigma)/P(-\sigma)$ of having a positive value of the time-averaged entropy production rate σ to that of having a negative value $-\sigma$, it does not give the functional form of the PDF $P(\sigma)$ itself [10,11]. More insights about fluctuations in the NESS can be obtained by examining the entropy production and irreversibility at the trajectory level [3,12].

To gain a better understanding of the NESS fluctuations in entropy production, several experimental studies have been carried out in a number of systems, including single Brownian particles in a trap moving at constant speed [13–15] or driven by a constant force across a periodic potential [3], power fluctuations in a vertically agitated granular gas [16], in liquid-crystal electroconvection [17], temperature and heat flux fluctuations in turbulent convection [18,19], and fluctuations of entropy production in driven RC-circuits [20–22]. These experiments provided new insights into the nature of nonequilibrium fluctuations. It is important to conduct the experiment in different physical systems, as one wants

*hillxgm@gmail.com

†pylai@phy.ncu.edu.tw

‡penger@ust.hk

to understand which aspects of the observed nonequilibrium fluctuations are universal and which are system specific. Such an understanding is needed for a large number of practical problems involving various complex NESS systems in material science, ecology, and biology.

Among the NESS systems that have been explored so far, colloidal monolayers suspended near a liquid-solid interface offer some unique advantages, because the dynamics of the particles are slower and can be tracked at the single-particle level with video microscopy [23]. They have served as model systems to study a range of interesting problems of phase transition kinetics and dynamics in two-dimensional (2D) soft matter systems [24,25].

Recently, we developed a two-layer colloidal system to study colloidal diffusion over a periodic potential [26]. The periodic potential is provided by the bottom colloidal spheres forming a crystalline pattern on a glass substrate. The corrugated surface of the colloidal crystal provides a gravitational potential field $U_0(x, y)$ for the diffusing particles on the top layer. Using optical microscopy, we measured the occupation statistics of the diffusing particles and constructed the potential $U_0(x, y)$ via the Boltzmann distribution. The dynamical properties of the diffusing particle, such as its escape time and diffusion coefficient, were simultaneously measured from the particle's trajectories. With the capability of simultaneously tracking the particle's motion at the single-particle level and measuring the external potential, the two-layer colloidal system provides a useful platform for the study of a range of interesting problems in nonequilibrium statistical physics.

For example, when the entire sample is tilted at an angle θ with respect to the vertical (gravity) direction, a tangential component of the gravitational force F is applied to the top-layer particles. In this case, DB is broken due to the presence of a steady particle flux, and the system is driven into a NESS. In a recent experiment [27], we measured the particle's mean drift velocity $v(F, E_b)$ and diffusion coefficient $D(F, E_b)$ as a function of F (by varying the tilt angle θ) and the energy barrier height E_b (by using different colloidal samples). The measured $v(F, E_b)$ and $D(F, E_b)$ agree well with the exact results of the 1D drift velocity [28] and diffusion coefficient [6,29]. Furthermore, for a tilted periodic potential, we measured the NESS probability density function (NESS-PDF) $P_{ss}(x, y)$, which deviates from the equilibrium distribution $P_B(x, y)$ to a different extent, depending on the driving or distance from equilibrium [30].

In this paper, we report a systematic study of the forward and reverse transition probability density functions (TPDFs) and entropy production in the NESS of the two-layer colloidal system. In the experiment, we measure the forward TPDF $\Pi(0, x, \tau)$ for a particle to move forward from its initial position 0 to its final position x over a lag time τ at various external forces F and the corresponding reverse TPDF $\Pi(x, 0, \tau)$. While both the measured $\Pi(0, x, \tau)$ and $\Pi(x, 0, \tau)$ show interesting space-time dependence, their ratio $\Pi(0, x, \tau)/\Pi(x, 0, \tau)$ is found to be independent of τ . In fact, the measured $\ln[\Pi(0, x, \tau)/\Pi(x, 0, \tau)]$ is found to be proportional to the tilted quasi-1D potential $U(x) = U_0(x) - Fx$, which is in excellent agreement with the theoretical prediction. This work thus provides a better understanding on how entropy is generated and heat is dissipated to the reservoir during a NESS transition

process. A major objective of this study is to delineate the experimental conditions for a precise measurement of the forward and reverse TPDFs and understand their effects in the NESS transition dynamics.

The paper is organized as follows. We first present, in Sec. II, the theory of 1D Brownian dynamics of individual particles in a tilted periodic potential. The experimental procedures and image processing methods are described in Sec. III. The experimental results and theoretical analysis are given in Sec. IV. Finally, the work is summarized in Sec. V.

II. THEORY

We study one-dimensional (1D) motion of a Brownian particle over a periodic potential $U_0(x) = U_0(x + \lambda)$, where λ is the period. When a constant force F is applied to the particle, the overall potential becomes $U(x) = U_0(x) - Fx$. The introduction of the external force F breaks the detailed balance condition and generates a net particle flux along the direction of F . We now consider the probability distribution function (PDF), $P(x, t)$, of finding a particle at position x and time t , whose initial space-time position is x_0 and t_0 . The 1D Smoluchowski equation for $P(x, t)$ reads [31]

$$\frac{\partial P(x, t)}{\partial t} = D_0 \frac{\partial^2 P(x, t)}{\partial x^2} + \frac{1}{\xi} \frac{\partial}{\partial x} \left(P(x, t) \frac{dU(x)}{dx} \right), \quad (3)$$

$$P(x, t_0) = \delta(x - x_0), \quad (4)$$

where $D_0 = k_B T / \xi$ is the particle's free diffusion coefficient with ξ being the friction coefficient and $k_B T$ the thermal energy. The first term on the right side of Eq. (3) is the diffusive flux density of the particle, and the second term is the convective flux density resulting from the conservative force $-dU(x)/dx$ acting on the particle. While an analytical time-dependent solution of the Smoluchowski equation is not available, one can numerically solve Eq. (3) under the initial condition Eq. (4). In this case, the solution $P(x_2, \tau)$ (with $\tau \equiv t - t_0$) becomes the transition probability density function (TPDF) $\Pi(x_1, x_2, \tau)$ (with $x_1 \equiv x_0$).

When the applied force $F = 0$, the system is at equilibrium without a net particle flux and the steady-state solution of Eq. (3) reduces to the Boltzmann distribution,

$$P_B(x) \sim e^{-U_0(x)/k_B T}. \quad (5)$$

In equilibrium, the transitions between any two positions are reversible because of the DB condition, which requires that the ratio of the forward TPDF to reverse TPDF follows the Boltzmann distribution as given by Eq. (2). It should be noted that the nonequilibrium nature of the TPDF $\Pi(x_1, x_2, \tau)$ [and $\Pi(x_2, x_1, \tau)$] is manifested in its explicit time dependence. In fact, in many cases, $\Pi(x_1, x_2, \tau)$ is a complicated function of delay time τ . The DB condition in Eq. (2) is nontrivial in that such complicated τ -dependence in $\Pi(x_1, x_2, \tau)$ [and $\Pi(x_2, x_1, \tau)$] cancels out exactly in the ratio of the forward TPDF to reverse TPDF and becomes an equilibrium Boltzmann factor. Equation (2) at equilibrium can be shown by the explicit calculations of $\Pi(x_1, x_2, \tau)$ using eigenfunction expansion of the Smoluchowski equation [32,33] or Onsager and Machlup (path integral) theory [34] and was verified experimentally in simple optical traps [33].

When a constant force $F \neq 0$ is applied to the Brownian particle, the system is driven into a NESS with a finite particle flux. In this case, the DB condition is expected to be broken; i.e., $P_{ss}(x_1)\Pi(x_1, x_2, \tau) \neq P_{ss}(x_2)\Pi(x_2, x_1, \tau)$. It was shown in a previous study [30] that the steady-state distribution $P_{ss}(x)$ in the periodic potential $U_0(x)$ has a non-Boltzmann form,

$$P_{ss}(x) = \frac{I_-(x)}{\frac{1}{\lambda} \int_0^\lambda dx I_-(x)}, \quad (6)$$

where

$$I_-(x) = \frac{1}{\lambda} \int_0^\lambda dy e^{-[U(x)-U(x+y)]/k_B T}. \quad (7)$$

Because of the spatial periodicity of the potential $U_0(x)$, the spatial coordinate of $P_{ss}(x)$ in Eq. (7) is defined in the domain $[0, \lambda]$ [30]. If one is interested in a spatial domain of several periods, say $m\lambda$ (where m is an integer ≥ 1), the steady-state distribution is simply given by $(1/m)P_{ss}(x)$.

Under the NESS condition, the energy input by the external force F acting on the Brownian particle is converted to the dissipated heat Q into the environment, giving rise to an increase in the total entropy:

$$\begin{aligned} \frac{S(x_1, x_2)}{k_B} &= \ln \left[\frac{P_{ss}(x_1)\Pi(x_1, x_2, \tau)}{P_{ss}(x_2)\Pi(x_2, x_1, \tau)} \right], \\ &= \ln \left[\frac{P_{ss}(x_1)}{P_{ss}(x_2)} \right] + \ln \left[\frac{\Pi(x_1, x_2, \tau)}{\Pi(x_2, x_1, \tau)} \right]. \end{aligned} \quad (8)$$

The total entropy production is thus decomposed into entropy productions in the system S_{sys} and environment (reservoir) S_{res} with

$$S_{sys} = k_B \ln \left[\frac{P_{ss}(x_1)}{P_{ss}(x_2)} \right] = -k_B [\ln P_{ss}(x_2) - \ln P_{ss}(x_1)] \quad (9)$$

being the entropy change of the particle (system) in going from $x_1 \rightarrow x_2$ and

$$S_{res} = k_B \ln \left[\frac{\Pi(x_1, x_2, \tau)}{\Pi(x_2, x_1, \tau)} \right]. \quad (10)$$

If the transition covers a distance greater than one period, i.e., $|x_2 - x_1|$ lies in the range $(m-1, m]$ for some integer $m \geq 1$, one should consider the spatial domain covering the m periods with $P_{ss} \rightarrow P_{ss}/m$. In this case, S_{sys} defined in Eq. (9) remains unchanged.

For NESS, although DB is broken, the ‘‘DB-like’’ relation in Eq. (2) still holds, i.e.,

$$\frac{\Pi(x_1, x_2, \tau)}{\Pi(x_2, x_1, \tau)} = e^{-[U(x_2)-U(x_1)]/k_B T}, \quad (11)$$

where $U(x) = U_0(x) - Fx$. Equation (11) can be proved using eigenfunction expansion of Eq. (3), as shown in the Appendix A. Note that Eq. (11) for the NESS case should not be confused with the DB condition at equilibrium, in which case the probability distribution is Boltzmann. Instead, Eq. (11) should be understood in terms of heat transfer under the NESS condition. With Eq. (11) and Eq. (10), we find

$$Q \equiv T S_{res} = -\Delta U_0 + F \Delta x, \quad (12)$$

where $\Delta U_0 = U_0(x_2) - U_0(x_1)$ and $\Delta x = x_2 - x_1$. Equation (11) thus can be understood in terms of the first law of

thermodynamics (conservation of energy), i.e., the work done by F to maintain the NESS is converted to the potential energy change ΔU_0 and heat Q dissipated into the reservoir.

With Eqs. (11) and (6), we obtain an analytic expression of the total entropy production

$$\frac{S(x_1, x_2)}{k_B} = \frac{F \Delta x}{k_B T} + \ln \left(\frac{\int_0^\lambda dy e^{[U_0(x_1+y)-Fy]/k_B T}}{\int_0^\lambda dy e^{[U_0(x_2+y)-Fy]/k_B T}} \right), \quad (13)$$

where $F \Delta x$ is the work done by the force F acting on a particle over a flat surface without a periodic potential. The second term on the right-hand side of Eq. (13) gives rise to oscillations about $F \Delta x / k_B T$ due to the spatially periodic potential $U_0(x)$. The entropy production of the particle itself (system) moving from x_1 to x_2 is given by

$$\frac{S_{sys}(x_1, x_2)}{k_B} = \frac{\Delta U_0}{k_B T} + \ln \left(\frac{\int_0^\lambda dy e^{[U_0(x_1+y)-Fy]/k_B T}}{\int_0^\lambda dy e^{[U_0(x_2+y)-Fy]/k_B T}} \right). \quad (14)$$

In the following sections, we will measure the forward and reverse transition probability density functions with the two-layer colloidal system and present the experimental verification of Eq. (11) and Eq. (13) for a tilted periodic potential.

III. EXPERIMENT

A. Apparatus and sample preparation

The experimental method and sample preparation used in this experiment are similar to those described in Refs. [27,30], and here we mention only some key points. Figure 1 shows the schematic of the sample cell, which is tilted at an angle θ with respect to the vertical (gravity) direction. The (dilute) colloidal particles on the top layer (blue) diffuse over the bottom colloidal crystal (red), which adheres to the glass substrate (GC). Polystyrene latex (PS) spheres (Thermo Scientific) of diameter $d_B = 5.2 \mu\text{m}$ are used for the bottom colloidal crystal. The procedures for cleaning the latex spheres and generating the bottom colloidal crystal have been described in Ref. [26]. After the formation of the colloidal crystal, the sample cell is filled with a 0.1 mM aqueous solution of NaCl followed by addition of a drop of colloidal suspension of silica

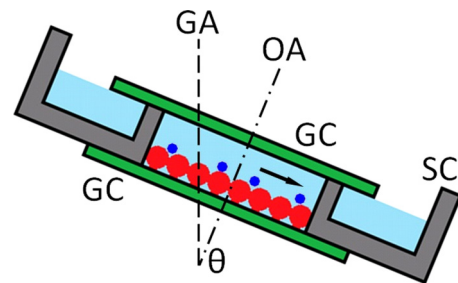


FIG. 1. Schematic diagram of the sample cell (side view): SC, stainless steel cell; GC, glass cover slip; GA, vertical (gravity) axis; OA, optical axis; θ , tilt angle of the sample cell; red particles, large polystyrene latex spheres forming a monolayer crystal on the bottom glass substrate; blue particles, smaller diffusing particles on top of the colloidal crystal; arrow, direction of the force F acting on the diffusing particles.

spheres of $d_T = 2.1 \mu\text{m}$ in diameter (Bangs laboratory). The silica spheres settle down on top of the bottom colloidal crystal and form a new layer of diffusing particles with a packing fraction n smaller than 0.1. The sample cell is then covered with a glass cover slip to prevent the solvent from evaporation.

The sample cell is placed on the stage of an inverted microscope (Leica DM-IRB), which is placed on a homemade incline with an adjustable tilt angle θ from 0 to 30° . With this setup, the external force F acting on the top-layer diffusing particles is given by $F = \Delta m g \sin(\theta)$, where Δm is the buoyant mass of the particle and g is the gravitational acceleration. Because Δm scales with d_T^3 , F depends strongly on the particle size. For the silica spheres used in this experiment, we find $F \simeq (0.05 \text{ pN}) \sin(\theta)$. The largest force that can be achieved with $\theta = 30^\circ$ is about 0.025 pN or $18F_T$ (with $F_T \equiv k_B T/\lambda$). Experimentally, F is determined via the equation $F = \xi v_0$, where $\xi = k_B T/D_0$ is the friction coefficient and v_0 is the drift velocity; both are measured over a flat incline [27]. In this way, F is determined without the need for calibrating θ and Δm .

B. Video microscopy and image analysis

The motion of the silica spheres is viewed with a $63\times$ oil-immersion objective and a $1.5\times$ relay lens. Movies of the particle motion are recorded under bright-field microscopy at a resolution of 1360×1024 pixels and at 30 frames per second using a monochrome CCD camera (Prosilica GC, Allied Vision). The focal plane of the objective is adjusted between the two layers of the particles, so that the image of the silica spheres is shown as bright spots over a honeycomb lattice of the bottom colloidal crystal. Figure 3 shows an example of the obtained microscope image. By applying a standard Gaussian image filter (MATLAB toolbox), we recover the Gaussian-like intensity profile of the diffusing particles. The center position of the intensity profile is thus chosen as the particle position. This method allows a repeatable tracking of particles with accuracy ~ 1 pixel or $\sim 70 \text{ nm}$. A MATLAB code based on the standard particle tracking algorithm [23] is used to find the trajectory of the diffusing particles.

C. Measurement of the transition probability density function (TPDF) $\Pi(x'_1, x'_2, \tau)$

As shown in Fig. 2, when the tilt force F is applied along the $[1,0]$ crystalline direction, the particle trajectories are essentially quasi-1D following a zigzag path as marked by the red line (which is shifted downward by $\lambda/2$ for clarity). Because of thermal fluctuations, the particle trajectories also show lateral fluctuations and occasional lateral transitions (in $[1,1]$ crystalline direction) to the nearby zigzag paths. To measure the longitudinal transitions parallel to F , we first filter out the trajectories containing the lateral transitions (in $[1,1]$ crystalline direction), so that the filtered trajectories all follow the same quasi-1D zigzag paths without changing lanes in the middle. The green curve in Fig. 2 shows an example of the filtered trajectory. To further filter out small lateral fluctuations along a fixed zigzag path, we project the actual particle trajectory $[x(t), y(t)]$ to the marked red zigzag line

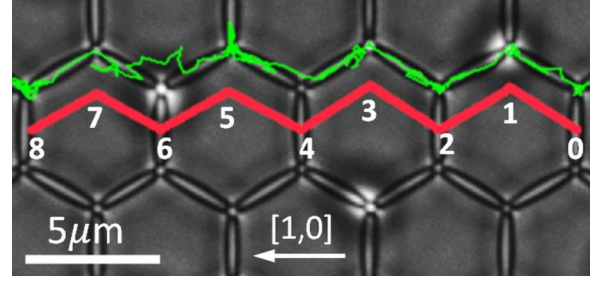


FIG. 2. Microscope image of top diffusing particles (white spots with a non-uniform intensity profile) over the bottom colloidal crystal (honeycomb pattern in the background). The green zigzag curve shows the measured particle trajectory. This 2D particle trajectory $[x(t), y(t)]$ is mapped to an equivalent quasi-1D trajectory $X(t)$, which is marked as the red zigzag line. For clarity, the red zigzag line is offset downward by $\lambda/2$. The integers 0 to 8 indicate the position of the sequential potential wells in $U_0(X)$ along the $[1,0]$ crystalline direction (white arrow). The scale bar is $5 \mu\text{m}$.

with the shortest normal distance to the zigzag line, and the particle position along the red zigzag line is denoted as $X(t)$.

Hereafter, we use the normalized coordinate $x' = X/\lambda$ to indicate the particle position. In this new coordinate system, the particle is at the local minimum of the potential wells in $U_0(x')$ when x' has an integer value, as shown in Fig. 2. Here $x' = 0$ is the local minimum position of the starting potential well. The TPDF is determined by $\Pi(x'_1, x'_2, \tau) = N/M$, where N is the number of trajectory segments starting at the position x'_1 and reaching to the position x'_2 over the delay time τ , and M is the total number of the trajectories with the same starting position x'_1 . To reduce the statistical error of the measured TPDFs, a bin size of $\lambda/10$ is used for averaging.

IV. RESULTS AND DISCUSSIONS

A. Forward transition probability density function (FTPDF) $\Pi(0, x', \tau')$

We first discuss the measurement of the forward transition probability density function (FTPDF) $\Pi(x'_1, x'_2, \tau)$ when a tilt force F is applied along the $[1,0]$ crystalline direction. In this case, the Brownian particles are driven into a NESS with a mean downward velocity v_d . The DB condition is broken, because $P_{ss}(x'_1)\Pi(x'_1, x'_2, \tau) > P_{ss}(x'_2)\Pi(x'_2, x'_1, \tau)$. As a result, the forward (downward) transitions are more frequent, spreading over multiple lattice periods (e.g., $x'_2 - x'_1 > 10$), and can be measured with good statistics. To simplify the notation, hereafter we choose the initial upstream position of the particle at $x'_1 = 0$ and its downstream position at $x'_2 \equiv x'$. The delay time τ is normalized as $\tau' = \tau/(\lambda/v_d)$.

Figure 3 shows a 3D plot of the measured FTPDF $\Pi(0, x', \tau')$ under a tilt force $F/F_T = 7.4$ along the $[1,0]$ crystalline direction. The lower-right region represents transitions over a large distance with a short delay time, whereas the upper-left region represents transitions over a very short distance (e.g., $< \lambda$) with a long delay time. These transitions are rare events and therefore the measured $\Pi(0, x', \tau')$ in these regions are close to zero (blank regions). The local peaks of the measured $\Pi(0, x', \tau')$ are the most probable transitions in

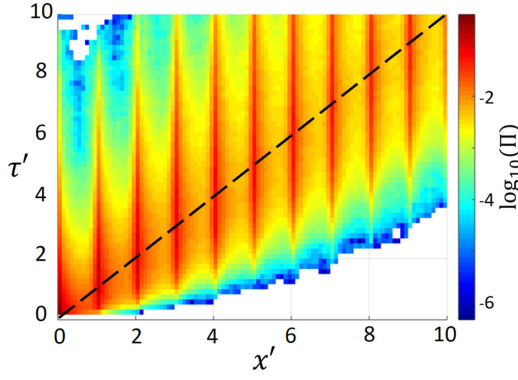


FIG. 3. 3D plot of the measured FTPDF $\Pi(0, x', \tau')$ under a tilt force $F/F_T = 7.4$ along the $[1,0]$ crystalline direction. Here the normalized distance $x' = X/\lambda$ and delay time $\tau' = \tau/(\lambda/v_d)$ are used in the plot (see text for details about their definitions). The values of $\Pi(0, x', \tau')$ are color-coded in log scale for better visualization. The black dashed line indicates $x' = \tau'$.

the x' - τ' plane. The black dashed line indicates the relation $x' = \tau'$, which passes through all the local peak positions of the measured $\Pi(0, x', \tau')$. This result suggests that the most probable values of $\Pi(0, x', \tau')$ describe a mean particle flow, which is determined by the equation $X = v_d \tau$.

Figure 4(a) shows the measured $\Pi(0, x', \tau')$ as a function of x' at four different values of delay time τ' . The FTPDF curves show repeated peaks at the locations where x' has integer values. The peak values of the measured $\Pi(0, x', \tau')$ at a fixed value of τ' can be described by a Gaussian-like

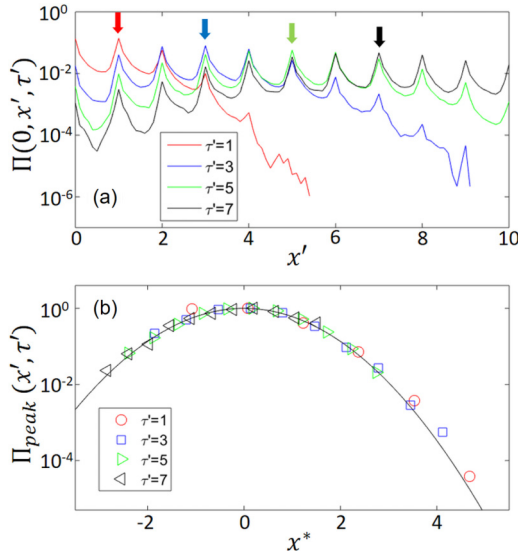


FIG. 4. (a) Measured FTPDF $\Pi(0, x', \tau')$ as a function of x' at four different values of the normalized delay time: $\tau' = 1$ (red), $\tau' = 3$ (blue), $\tau' = 5$ (green), and $\tau' = 7$ (black). The arrows point to the global maximal position in each curve with the same color code. (b) Replot of the peak values of the measured $\Pi(0, x', \tau')$ in (a) as a function of the normalized transition distance, $x^* = (X - v_d \tau)/(2D\tau)^{1/2}$. The color code used for the data points is the same as that in (a). The solid line shows the fitting of Eq. (15) to the data points with $v_d = 0.14 \mu\text{m/s}$ and $D = 0.17 \mu\text{m}^2/\text{s}$.

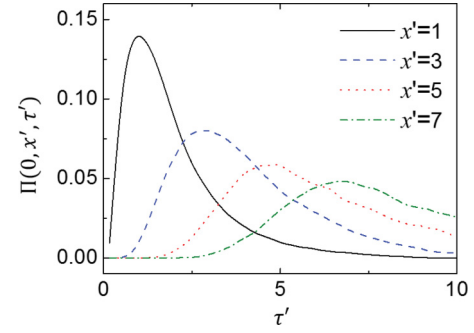


FIG. 5. Measured FTPDF $\Pi(0, x', \tau')$ as a function of τ' at four different values of transition distance: $x' = 1$ (black), $x' = 3$ (blue), $x' = 5$ (red), $x' = 7$ (green). These are the locations of the local minimum of the potential wells in $U_0(x')$.

envelop function $\Pi_{\text{peak}}(x', \tau')$, which has a global maximum at the location x'_{max} . The value of x'_{max} , which is pointed by an arrow for each value of τ' , is found to increase with τ' . To show this envelop function more clearly, we replot of the peak values of $\Pi(0, x', \tau')$, in Fig. 4(b), as a function of the normalized transition distance, $x^* = (X - v_d \tau)/(2D\tau)^{1/2}$. Here v_d and D are, respectively, the mean downward velocity and diffusion coefficient of the particles under the tilt force F . Using the same procedures as described in Ref. [27], we find $v_d = 0.14 \pm 0.02 \mu\text{m/s}$ and $D = 0.15 \pm 0.05 \mu\text{m}^2/\text{s}$ from the obtained particle trajectories. It is seen that all the data points collapse onto a master curve, once the normalized transition distance x^* is used. The master curve is well described by a Gaussian function,

$$\Pi_{\text{peak}}(X, \tau) = \frac{\Pi_0}{\sqrt{2D\tau}} e^{-\frac{1}{2} \left(\frac{X - v_d \tau}{\sqrt{2D\tau}} \right)^2}, \quad (15)$$

where Π_0 is a normalization constant. The solid line in Fig. 4(b) shows the fitting of Eq. (15) to the data points with $v_d = 0.14 \mu\text{m/s}$ and $D = 0.17 \mu\text{m}^2/\text{s}$. The fitted values of v_d and D agree well with the experimental results, as mentioned above.

Figure 5 shows the measured $\Pi(0, x', \tau')$ as a function of τ' at four different values of x' . These FTPDF curves have a single peak with the peak position satisfying the condition $\tau' = x'$, as mentioned above. The peak amplitude is found to decrease monotonically with x' . These features are consistent with the prediction of Eq. (15). Figures 3–5 thus reveal that the forward transitions of the particles contain a combined motion of a mean drift together with some random diffusion.

Based on the above findings, we speculate that the FTPDF $\Pi(0, x', \tau')$ may have the following approximate form:

$$\Pi(0, x', \tau') \simeq g(x') \Pi_{\text{peak}}(x', \tau'), \quad (16)$$

where the large-scale gross feature of the FTPDF is described by the envelop function $\Pi_{\text{peak}}(x', \tau')$ given in Eq. (15), and the local fine details are modulated by some rapid varying function $g(x')$ describing the spatial variations. For a flat incline with $U(x) = -Fx$, Eq. (16) gives the exact solution with $g(x') = 1$. Although there is no analytic closed form solution available for the time-dependent Smolouchowski equation [Eq. (3)], Eq. (16) serves as a convenient approximation. In particular, by fitting the measured $\Pi(0, x', \tau')$ in Fig. 3 to Eq. (16), we

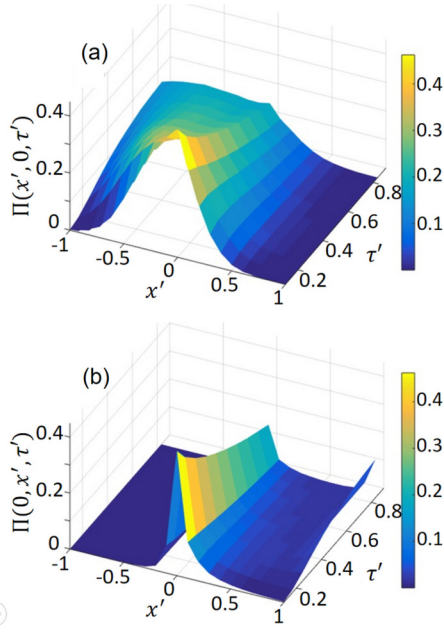


FIG. 6. (a) 3D plot of the measured reverse TPDF $\Pi(x', 0, \tau')$ as a function of x' and τ' under a tilt force $F/F_T = 3.7$ along the $[1, 0]$ crystalline direction. (b) 3D plot of the measured forward TPDF $\Pi(0, x', \tau')$ under the same condition as that in (a).

find that $g(x')$ has a form very close to the measured $P_{ss}(x')$ as shown in Fig. 8 below. The approximation in Eq. (16) is further justified in Appendix B.

B. Reverse to forward TPDF ratio $\Pi(x', 0, \tau')/\Pi(0, x', \tau')$

For a tilt potential, the reverse (upward) transitions are much less frequent than the downward transitions. To accurately measure the reverse TPDF $\Pi(x', 0, \tau')$, we use a small tilt force F so that one can have enough statistics for the upward transitions. Figures 6(a) and 6(b) show, respectively, the 3D plot of the measured reverse TPDF $\Pi(x', 0, \tau')$ and forward TPDF $\Pi(0, x', \tau')$ under the same condition with $F/F_T = 3.7$. With this small force, upward transitions over two periods (i.e., $x' = 2$) can be observed but their occurrence is rare. No particle is observed to have an upward transition for more than three periods. Therefore, the measured $\Pi(x', 0, \tau')$ is presented only in the ranges of $-1 \leq x' \leq 1$ and $-1 \leq \tau' \leq 1$ with adequate statistics. Because of the finite size ($\lambda/10$) of the binning in x' , the peak value $\Pi(0, 0, 0)$ ($\simeq 0.46$) is smoothed out to about its half expected value. Nevertheless, this systematic error becomes negligibly small at large values of x' and is canceled out mostly in the measured TPDF ratio $\Pi(0, x', \tau')/\Pi(x', 0, \tau')$.

Figure 7(a) shows a 3D plot of the measured log ratio, $\ln[\Pi(x', 0, \tau')/\Pi(0, x', \tau')]$, of the reverse TPDF $\Pi(x', 0, \tau')$ to the forward TPDF $\Pi(0, x', \tau')$ as a function of x' and τ' . Along the τ' axis, the data surface shows little variation, despite that both the measured $\Pi(x', 0, \tau')$ and $\Pi(0, x', \tau')$ have a strong τ -dependence, as shown in Figs. 3 and 5. Along the x' axis, the measured $\ln[\Pi(x', 0, \tau')/\Pi(0, x', \tau')]$ changes very much like a tilted periodic potential. To further verify these features, we show, in Fig. 7(b), the 1D-plot of the measured $\ln[\Pi(x', 0, \tau')/\Pi(0, x', \tau')]$ as a function of x' for 5 different

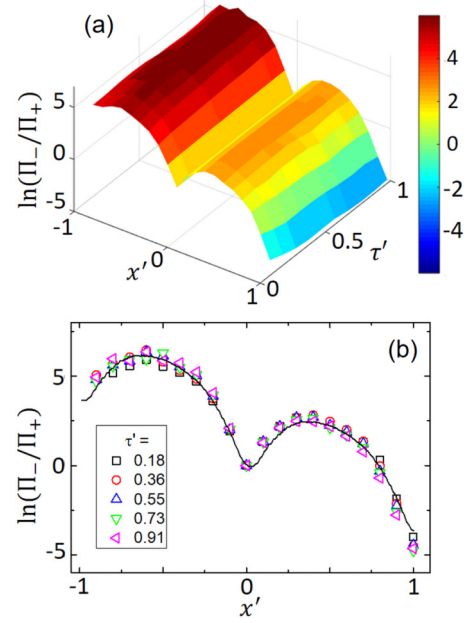


FIG. 7. (a) 3D plot of the measured log ratio $\ln(\Pi_-/\Pi_+)$ of the reverse TPDF $\Pi_- \equiv \Pi(x', 0, \tau')$ to the forward TPDF $\Pi_+ \equiv \Pi(0, x', \tau')$ under a tilt force $F/F_T = 3.7$ along the $[1, 0]$ crystalline direction. (b) 1D plot of the measured $\ln(\Pi_-/\Pi_+)$ as a function of x' at 5 different values of delay time: $\tau' = 0.18$ (black squares), $\tau' = 0.36$ (red circles), $\tau' = 0.55$ (blue up triangles), $\tau' = 0.73$ (green down triangles), and $\tau' = 0.91$ (pink left triangles). The black line is a plot of Eq. (11) with the measured tilted potential $U(x')$.

values of delay time τ' . It is seen that all the data points with different values of τ' collapse onto the same master curve, suggesting that the measured $\Pi(x', 0, \tau')/\Pi(0, x', \tau')$ is indeed independent of the delay time τ' . Furthermore, the data set is found to be well described by the measured tilted potential $U(x') = U_0(x') - Fx'$ (solid line), where $U_0(x')$ is the untilted potential shown in Figure 8 below. Figure 7 thus verifies Eq. (11) for the NESS, which provides a new way to reconstruct the potential $U(x)$ [and hence $U_0(x')$] from the measured $\Pi(x', 0, \tau')/\Pi(0, x', \tau')$.

C. Total entropy production $S(0, x')$

To calculate the total entropy production $S(0, x')$ in Eq. (8), one needs to measure the NESS PDF $P_{ss}(x')$ in addition to the transition probabilities. The method of measuring $P_{ss}(x')$ has been described in Ref. [30], and here we only present the final results. Figure 8(a) shows the measured quasi-1D equilibrium PDF $P_B(x')$ for a leveled sample with $F = 0$. The measured $P_B(x')$ is normalized so that the sum of $P_B(x')$ within one period is equal to unity. The inset shows the equilibrium potential $U_0(x')/k_B T = -\ln[P_B(x')]$ obtained using Eq. (5). The energy barrier between the two neighboring potential wells is $E_b \simeq 4.0k_B T$. We numerically fit the measured $U_0(x')$ with a smooth solid line and use it to calculate other quantities to be discussed below.

Figures 8(b) and 8(c) show, respectively, the measured $P_{ss}(x')$ under the tilt force $F/F_T = 3.7$ and $F/F_T = 7.4$. Here $P_{ss}(x')$ is also normalized so that the total probability within

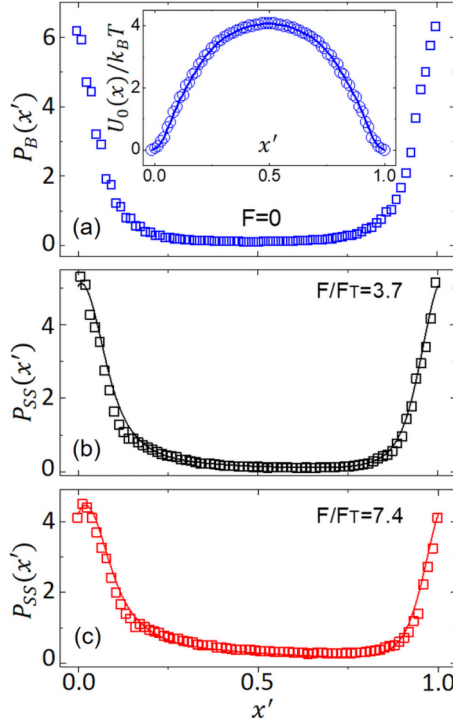


FIG. 8. (a) Measured quasi-1D equilibrium PDF $P_B(x')$ as a function of x' . The measurement is made for a leveled sample with the external force $F = 0$. Inset shows the equilibrium potential $U_0(x')/k_B T = -\ln[P_B(x')]$ (blue circles) obtained using Eq. (5). The solid line is a smooth fitting curve of $U_0(x')$. (b, c) Measured quasi-1D NESS-PDF $P_{ss}(x')$ as a function of x' (open squares) under two different tilt forces along the $[1,0]$ direction: (b) $F/F_T = 3.7$ and (c) $F/F_T = 7.4$. The solid lines are the numerical results calculated using Eq. (6) with the measured potential $U_0(x')$ in (a).

one period equals to unity. In contrast to the equilibrium PDF $P_B(x')$, the measured NESS-PDF $P_{ss}(x')$ becomes more and more asymmetric with increasing values of F . More details about the evolution of the measured $P_{ss}(x')$ with increasing F along the $[1,0]$ direction have been described in Ref. [30]. We numerically calculate $P_{ss}(x')$ using Eq. (6) with the measured potential $U_0(x')$ in Fig. 8(a) and the final results are shown as the solid lines in Figs. 8(b) and 8(c). An excellent agreement between the experiment and numerical calculation is found, further confirming that Eq. (6) and the quasi-1D approach used here are accurate for the experiment.

With the measured $P_{ss}(x')$ and transition probabilities, we calculate the total entropy production $S(0,x')$ using Eq. (8). Figure 9 shows the obtained $S(0,x')$ as a function of x' under two different values of F . For a flat incline with the periodic potential $U_0(x') = 0$, one expects the work done by the tilt force F leads to the entropy production of $(F/F_T)x'$, which is shown by the dashed lines. For a finite $U_0(x') \neq 0$, $S(0,x')$ increases monotonically with x' , but the entropy production is small if the transition occurs in regions around the local minimum of $U_0(x')$. However, the entropy production over one period is independent of $U_0(x')$ and is given by $F\lambda/T$. Because the mean transition time for one period is $\bar{\tau} = \lambda/v_d$, the mean entropy production rate is thus given by $(F\lambda/T)/\bar{\tau} = (Fv_d)/T$. Similar patterns of entropy production

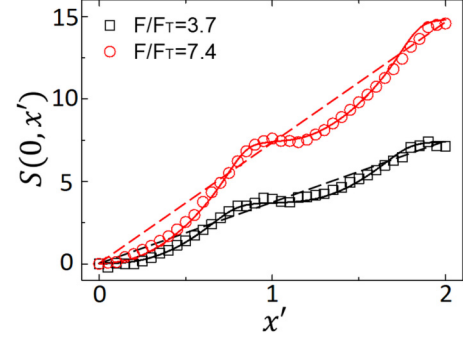


FIG. 9. Measured total entropy production $S(0,x')$ under two different tilt forces along the $[1,0]$ direction: $F/F_T = 3.7$ (black squares) and $F/F_T = 7.4$ (red circles). The solid lines are the numerical results calculated using Eq. (13). The dashed lines show the work $(F/F_T)x'$ done by F over the distance x' .

were also found in a recent numerical study [5]. One can also numerically calculate $S(0,x')$ using Eq. (13) together with the measured $U_0(x')$ and $P_{ss}(x')$. The solid lines in Fig. 9 show the numerically calculated $S(0,x')$, which agree well with the experimental results.

It is seen that the measured $S(0,x')$ changes slowly with respect to x' near the potential wells (where $x' = 0, 1, 2$), and then its slope rises significantly in the second half period (e.g., $0.5 < x' < 1$). The changing slope in $S(0,x')$ suggests that the entropy is not uniformly produced within a single period of $U_0(x')$, revealing a fine structure of dissipation in a NESS. Near the potential wells where the local entropy production gradient, $\Delta S(0,x')/\Delta x'$, almost vanishes, the particles are almost at thermal equilibrium where most work done by F is stored in the potential and little is converted to heat. This statement is consistent with the fact that the fraction of particles contributing to the mean flux reaches its minimal value near the potential wells. In contrast, the maximal entropy production gradient is found where $U_0(x')$ declines the fastest. In this region (i.e., on the downward side of the potential barrier), both the work done by F and potential energy stored in the first half period of $U_0(x')$ are converted to heat, which is dissipated into the environment. Also, the fraction of particles contributing to the mean flux reaches its maximal value.

V. SUMMARY

We have carried out a systematic study of the forward and reverse transition probabilities and entropy production in a NESS. The NESS is realized in a two-layer colloidal system, in which the bottom-layer colloidal crystal provides a 2D periodic potential $U_0(x,y)$ for the top-layer diffusing particles. By tilting the sample cell at an angle θ with respect to gravity, a tangential component of the gravitational force F is applied to the diffusing particles, and the tilted potential $U(x) = U_0(x) - Fx$ is effectively quasi-1D along the $[1,0]$ crystalline orientation. The applied force F breaks the detailed balance (DB) condition and generates a steady particle flux along the $[1,0]$ direction. This is a well-characterized system, which has been employed recently to study the diffusive and force-assisted barrier crossing dynamics of colloidal particles [26,27,30].

In this work, we measured the forward transition probability density function $\Pi(0,x,\tau)$ at various values of F and the corresponding reverse transition probability density function $\Pi(x,0,\tau)$. The measured FTPDF $\Pi(0,x,\tau)$ has a complex functional form with repeated peaks along the x axis. The values of these peaks are well described by a Gaussian-like envelop function given in Eq. (15). While both the measured $\Pi(0,x,\tau)$ and $\Pi(x,0,\tau)$ show interesting space-time dependence, their ratio $\Pi(0,x,\tau)/\Pi(x,0,\tau)$ is found to be independent of τ and obey a DB-like relation as shown in Eq. (11). Indeed, the measured $\ln[\Pi(0,x,\tau)/\Pi(x,0,\tau)]$ is found to be proportional to the tilted potential $U(x)$, which is in excellent agreement with the theoretical prediction. Our theoretical analysis assumed that the colloidal motion is over-damped, which holds for the current experiment. For under-damped diffusion in which the inertial effect may be important, one expects that Eq. (11) still holds when the delay time is much larger than the damping relaxation, i.e., when $\tau \gg m/\xi$, where m is the mass and ξ is the friction coefficient of the particles. When the inertial effect becomes important, one anticipates corrections to Eq. (11), which can be investigated in a future study.

Furthermore, we measured the probability density function (NESS-PDF) $P_{ss}(x)$ and total entropy production $S(0,x)$ in the NESS. The measured $S(0,x)$ is found to increase linearly with the traveling distance x and is superimposed with a periodic modulation by the potential $U_0(x)$. Our theoretical calculations reveal that the DB-like relation in Eq. (11) is inherently linked to the heat transfer between the diffusing particles and environment under the NESS condition, namely, the work done by the external fore F to maintain the NESS is converted to the potential energy change $U_0(x)$ and heat Q dissipated into the reservoir. This work thus provides a better understanding on how entropy is generated and heat is dissipated to the reservoir during a NESS transition process. It also demonstrates the applications of the two-layer colloidal system in the study of NESS transition dynamics. With a fine control of the functional form of the external force F , one can also use the well-characterized colloidal system to study a range of interesting problems in non-equilibrium statistical physics beyond NESS.

ACKNOWLEDGMENTS

This work was supported in part by RGC of Hong Kong SAR under Grants No. HKUST16302816 (P.T.) and No. AoE/P-02/12 (P.T.), and by the MoST of Taiwan under Grant No. 104-2112-M-008-003-MY3 (P.Y.L.).

APPENDIX A: DERIVATION OF EQ. (11) FOR NESS

For convenience, here we use dimensionless units. Since there is no explicit time dependence in the right hand side of the Smoluchowski equation [Eq. (3)], one can use the separation ansatz $P(x,t) = \varphi(x)e^{-\lambda t}$ and obtain the eigenvalue problem

$$\mathbf{L}_S \varphi_n \equiv \partial_x(\partial_x + U'(x))\varphi_n = -\lambda_n \varphi_n, \quad (\text{A1})$$

where the eigenvalues and eigenfunctions depend on the boundary conditions, and the Smoluchowski operator \mathbf{L}_S is non-Hermitian. However, the Smoluchowski equation can be

transformed to the Schrödinger equation with a potential $V(x)$, which has the same eigenvalues (under the same boundary conditions) via [35]

$$\begin{aligned} \psi(x) &\equiv e^{\frac{U(x)}{2}} \varphi(x), \\ V(x) &\equiv \frac{[U'(x)]^2}{4} - \frac{U''(x)}{2}, \\ \mathbf{L}\psi_n &\equiv (\partial_x^2 - V(x))\psi_n = -\lambda_n \psi_n. \end{aligned} \quad (\text{A2})$$

Here the Schrödinger operator \mathbf{L} is Hermitian and so all eigenvalues λ_n are real. The Schrödinger eigenfunctions satisfy the usual orthonormality and completeness conditions,

$$\begin{aligned} \int dx \psi_n(x) \psi_m(x) &= \delta_{mn}, \\ \sum_n \psi_n(x) \psi_n(x') &= \delta(x - x'). \end{aligned} \quad (\text{A3})$$

The PDF $P(x,t)$ can then be expanded by the eigenfunctions as

$$P(x,t) = \sum_n c_n e^{-\lambda_n t} \varphi_n(x) = e^{-\frac{U(x)}{2}} \sum_n c_n e^{-\lambda_n t} \psi_n(x). \quad (\text{A4})$$

Suppose the initial position of the particle located sharply at $x = a$, i.e., $P(x,0) = \delta(x - a)$, then from the completeness and orthonormal conditions, one gets $c_n = e^{U(a)/2} \psi_n(a)$ and hence the eigenfunction expansion solution is

$$P(x,t) = \Pi(a \rightarrow x, t) = e^{\frac{U(a)-U(x)}{2}} \sum_n e^{-\lambda_n t} \psi_n(x) \psi_n(a). \quad (\text{A5})$$

Similarly, if the particle is initially at x , the probability for it to transit to a in time t is given by

$$\Pi(x \rightarrow a, t) = e^{\frac{U(x)-U(a)}{2}} \sum_n e^{-\lambda_n t} \psi_n(x) \psi_n(a). \quad (\text{A6})$$

Taking the ratio of the forward and reverse transition probabilities in the above two equations gives Eq. (11). It can also be shown that Eq. (11) holds for NESS using the Langevin equation and Onsager-Machlup approach [7,33].

APPENDIX B: DERIVATION OF THE APPROXIMATE EQ. (16)

Again for convenience, we use dimensionless units here. Starting from the 1D Smoluchowski equation for $P(x,t)$ given by

$$\partial_t P = \partial_x \left(\partial_x P + P(x,t) \frac{dU(x)}{dx} \right), \quad (\text{B1})$$

our goal is to show or justify that $P(x,t) \approx P_0(x,t) \times P_{ss}(x)$, where we shall show that $P_0(x,t)$ can be approximately described by the forced diffusion equation (under the force $f \equiv F\lambda/k_B T$) whose solution is a drifted Gaussian in analogy to Π_{peak} in Eq. (15).

Assuming the ansatz $P(x,t) = P_0(x,t)P_{ss}(x)$ and substituting it into Eq. (B1), and using the steady-state (constant) flux

$v = -P'_{ss} - P_{ss}U'$, one gets

$$\begin{aligned} P_{ss}\partial_t P_0(x,t) &= \partial_x(P_{ss}\partial_x P_0 + P_0 P'_{ss} + P_0 P_{ss}U') \\ &= P_{ss}\partial_x^2 P_0 + (P'_{ss} - v)\partial_x P_0, \end{aligned} \quad (\text{B2})$$

$$\Rightarrow \partial_t P_0(x,t) = \partial_x^2 P_0 + \frac{P'_{ss} - v}{P_{ss}} \partial_x P_0. \quad (\text{B3})$$

Now we make the approximation for the coefficient of $\partial_x P_0$ in Eq. (B3) by its average over one period. This is justified since P_0 describes the large-scale behavior of $P(x,t)$ and should not be very sensitive to the local variations within one period. In this case, we have

$$\frac{P'_{ss} - v}{P_{ss}} \simeq \int_0^1 \frac{P'_{ss}(x) - v}{P_{ss}(x)} dx = -v \int_0^1 \frac{dx}{P_{ss}(x)} = -f, \quad (\text{B4})$$

where the last equality follows from the potential reconstruction formula under the NESS condition [30],

$$U(x) - U(0) = -\ln \frac{P_{ss}(x)}{P_{ss}(0)} - v \int_0^x \frac{du}{P_{ss}(u)}. \quad (\text{B5})$$

As a result, Eq. (B3) can be approximated by the forced diffusion equation

$$\partial_t P_0(x,t) = \partial_x^2 P_0 - f \partial_x P_0, \quad (\text{B6})$$

where the effect of the external potential $U_0(x)$ is ignored. The solution of Eq. (B6) is a drifted Gaussian similar to that shown in Eq. (15).

-
- [1] F. Reif, *Fundamentals of Statistical and Thermal Physics* (McGraw-Hill, Auckland, 1985).
- [2] R. Zia and B. Schmittmann, *J. Phys. A: Math. Gen.* **39**, L407 (2006).
- [3] T. Speck, V. Blickle, C. Bechinger, and U. Seifert, *Europhys. Lett.* **79**, 30002 (2007).
- [4] D. Ruelle, *Phys. Today* **57**, 48 (2004).
- [5] P. Pietzonka, E. Zimmermann, and U. Seifert, *Europhys. Lett.* **107**, 20002 (2014).
- [6] P. Reimann, C. Van den Broeck, H. Linke, P. Hanggi, J. M. Rubi, and A. Perez-Madrid, *Phys. Rev. E* **65**, 031104 (2002).
- [7] R. D. Astumian, *Phys. Chem. Chem. Phys.* **9**, 5067 (2007).
- [8] D. J. Evans, E. G. D. Cohen, and G. P. Morriss, *Phys. Rev. Lett.* **71**, 2401 (1993).
- [9] G. Gallavotti and E. G. D. Cohen, *Phys. Rev. Lett.* **74**, 2694 (1995).
- [10] D. J. Evans and D. J. Searles, *Adv. Phys.* **51**, 1529 (2002).
- [11] U. Seifert, *Rep. Prog. Phys.* **75**, 126001 (2012).
- [12] K. H. Chiang, C. L. Lee, P. Y. Lai, and Y. F. Chen, *Phys. Rev. E* **95**, 012158 (2017).
- [13] D. Andrieux, P. Gaspard, S. Ciliberto, N. Garnier, S. Joubaud, and A. Petrosyan, *Phys. Rev. Lett.* **98**, 150601 (2007).
- [14] D. M. Carberry, J. C. Reid, G. M. Wang, E. M. Sevick, D. J. Searles, and D. J. Evans, *Phys. Rev. Lett.* **92**, 140601 (2004).
- [15] G. M. Wang, D. M. Carberry, J. C. Reid, E. M. Sevick, and D. J. Evans, *J. Phys.: Condens. Matter* **17**, S3239 (2005).
- [16] K. Feitosa and N. Menon, *Phys. Rev. Lett.* **92**, 164301 (2004).
- [17] W. I. Goldburg, Y. Y. Goldschmidt, and H. Kellay, *Phys. Rev. Lett.* **87**, 245502 (2001).
- [18] S. Ciliberto and C. Laroche, *J. Phys. IV France* **8**, Pr6-215 (1998).
- [19] X.-D. Shang, P. Tong, and K.-Q. Xia, *Phys. Rev. E* **72**, 015301(R) (2005).
- [20] R. van Zon, S. Ciliberto, and E. G. D. Cohen, *Phys. Rev. Lett.* **92**, 130601 (2004).
- [21] S. Ciliberto, A. Imparato, A. Naert, and M. Tanase, *Phys. Rev. Lett.* **110**, 180601 (2013).
- [22] K. H. Chiang, C. W. Chou, C. L. Lee, P. Y. Lai, and Y. F. Chen, *Europhys. Lett.* **113**, 30001 (2016).
- [23] J. C. Crocker and D. G. Grier, *J. Colloid Interface Sci.* **179**, 298 (1996).
- [24] P. N. Pusey, in *Liquids, Freezing and Glass Transition*, edited by J. P. Hansen, D. Levesque, and J. Zinn-Justin (North-Holland, Amsterdam, 1991), Chap. 10.
- [25] B. P. Binks and T. Horozov, *Colloidal Particles at Liquid Interfaces* (Cambridge University Press, Cambridge, UK, 2006).
- [26] X. G. Ma, P. Y. Lai, and P. Tong, *Soft Matter* **9**, 8826 (2013).
- [27] X.-G. Ma, P.-Y. Lai, B. J. Ackerson, and P. Tong, *Soft Matter* **11**, 1182 (2015).
- [28] R. L. Stratonovich, *Radiotekh. Elektron.* **3**, 497 (1958).
- [29] P. Reimann, C. Van den Broeck, H. Linke, P. Hanggi, J. M. Rubi, and A. Perez-Madrid, *Phys. Rev. Lett.* **87**, 010602 (2001).
- [30] X.-G. Ma, P.-Y. Lai, B. J. Ackerson, and P. Tong, *Phys. Rev. E* **91**, 042306 (2015).
- [31] W. B. Russel, D. A. Saville, and W. R. Schowalter, *Colloidal Dispersions* (Cambridge University Press, Cambridge, 1989).
- [32] M. Doi and S. F. Edwards, *Theory of Polymer Dynamics* (Oxford Press, Oxford, 1988).
- [33] M. N. P. Confesor and P.-Y. Lai, *Chin. J. Phys.* **51**, 522 (2013).
- [34] M. Bier, I. Derenyi, M. Kostur, and R. D. Astumian, *Phys. Rev. E* **59**, 6422 (1999).
- [35] H. Risken, *The Fokker-Planck Equation*, 2nd ed. (Springer, Berlin, 1998), Sec. 5.4.